XLVI CILAMCE
VITÓRIA - ES - BRAZIL - 2025
XLVI IBERO-LATIN AMERICAN CONGRESS ON COMPUTATIONAL METHODS IN ENGINEERING

Direct Strength Method Design of CFS Lipped Channel Beams under Fire-Induced Distortional and Global Buckling Modes

Natan Sian das Neves[1], Alexandre Landesmann[1], Dinar Camotim[2]

[1] *Programa de Engenharia Civil, PEC/COPPE/UFRJ, Universidade Federal do Rio de Janeiro*
Av. Athos da Silveira Ramos-149. Centro de Tecnologia – Bloco B, Sala 101, 21941-909, Rio de Janeiro, Brasil
natan.neves@coc.ufrj.br, alandes@coc.ufrj.br
[2] *CERIS, DECivil, Instituto Superior Técnico, Universidade de Lisboa*
Av. Rovisco Pais, 1049-001, Lisboa, Portugal
dcamotim@civil.ist.utl.pt

Abstract. This work reports the findings of a comprehensive numerical investigation on the post-buckling behaviour, failure and Direct Strength Method (DSM) design of cold-formed steel (CFS) single-span simply supported lipped channel beams buckling in pure distortional and global modes at elevated temperatures (up to 800 ºC) due to fire conditions. It extends the scope of a previous investigation carried out by Landesmann and Camotim [1], by analysing a substantially larger lipped channel beam set, exhibiting various cross-section dimensions and yield stresses, selected to cover wider distortional slenderness ranges. The beams analysed (i) display two end support conditions (SCA and SCB), (ii) the Eurocode 3 (part 1.2) model to describe the temperature-dependence of the CFS material properties is adopted and (iii) the results are obtained by means of ABAQUS shell finite element GMNIA. After presenting and discussing the main features of the beam distortional and global post-buckling behaviour, extensive beam failure moment sets are gathered and used to develop and validate DSM-based design approaches. The methodology followed consists of modifying the most performant available DSM-based design curves, which naturally involves the temperature-dependent reduction factors of the CFS model. A merit assessment procedure shows that the modified DSM-based strength curves predict the lipped channel beam distortional and global failure moments with remarkable accuracy and reliability, thus constituting an excellent starting point to search for a DSM-based design approach capable of handling arbitrary CFS beams failing in pure distortional and global modes at elevated temperatures.

Keywords: Cold-formed steel beams, Elevated temperatures, Distortional and Global post-buckling behaviour, Shell finite element analysis, Direct Strength Method (DSM) design.

1 Introduction

Cold-formed steel (CFS) structures are widely employed due to their high strength-to-weight ratio, manufacturing flexibility, and competitive production and assembly costs, making them a compelling solution for efficient and versatile structural applications. However, the slender geometry of open-section thin-walled CFS members makes them particularly vulnerable to instability phenomena, including local, distortional, and global buckling modes. To mitigate such vulnerabilities, current design standards incorporate specific provisions aimed at ensuring structural reliability. Among the available design methodologies, the Direct Strength Method (DSM) has gained broad international recognition—being adopted in North American, Australian/New Zealand, and Brazilian specifications [1-6] – for its rational foundation and practical implementation, which relies solely on the evaluation of member yield and critical buckling stresses. The objective of this study is to extend the work of Martins *et al*. [7] and Kankanamge and Mahendran [8] by investigating cold-formed steel beams subjected to uniform major-axis bending and failing through distortional (D) or global (lateral-torsional – LT) buckling, under elevated temperature conditions representative of fire scenarios. The analysis addresses (i) the temperature-dependent buckling, post-buckling and ultimate strength behaviour of such members, and (ii) the development and calibration of DSM-based design formulations suitable for structural fire design.

2 Buckling behaviour – beam geometry selection

As done in previous studies (*e.g.*, [7, 9]), the first task of this work consists of selecting the geometries (cross-section dimensions and lengths) of the single-span CFS lipped channel beams to be analysed. Two end support conditions are considered, denoted here SCA and SCB [9], both simply supported with respect to major and minor-axis bending and having the end cross-section torsional rotations prevented – the difference resides in the fact that the end cross-section warping and local displacements and rotations are either free (SCA beams – unrestrained end cross-sections) or fully prevented (SCB beams – rigid plates are attached to their end cross-sections) – Figs. 1(a)-(b) depict the differences between these two support conditions. The selection procedure involves sequences of buckling analyses, performed by means of the code GBTUL [10] (based on Generalized Beam Theory – GBT) or ABAQUS SFEA and intended to identify beams buckling and failing in "pure" distortional and global modes.

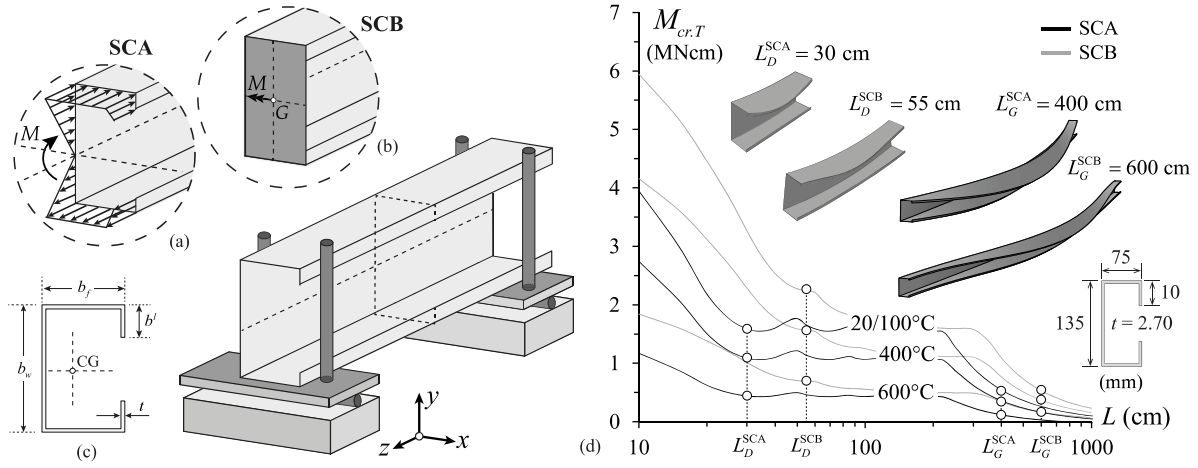


Figure 1. (a) SCA and (b) SCB lipped channel beams end support and loading conditions, (c) LC geometry and dimensions and (d) variation of $M_{cr.T}$ with L and T=20/100, 400 and 600°C for SCA and SCB LC beams (135×75×10×2.70 mm), adopting the EC3-1.2 [11] CFS constitutive model

The end product of the lipped channel beams selection procedure is the 30 and 21 cross-section dimensions (b_w, b_f, b_l and t – see Fig. 1(c)) given in [7, 9]. The $M_{cr.T}$ vs. L curves depicted in Fig. 1(d) provide the variation of the critical buckling moment at temperature with the length L (logarithmic scale) and temperature T, for SCA and SCB beams with the LC cross-section (135×75×10×2.70 mm), and (ii) the EC3-1.2 [11] constitutive model is adopted. Also shown are the critical (distortional and global) buckling modes of the SCA beam with L_D^{SCA} = 30 cm and L_G^{SCA} = 400 cm, and SCB beam with L_D^{SCB} = 55 cm and L_G^{SCB} = 600 cm. It should be pointed out that any given buckling curve can be obtained through a "vertical translation" of the top one, with a magnitude depending solely on the Young's modulus erosion stemming from the temperature rise. Moreover, the critical distortional and global moment corresponds to the same length (L_D and L_G) for all temperature values.

3 Beam Post-Buckling Behaviour

3.1 Numerical model

The beam post-buckling equilibrium paths and failure moments were determined through ABAQUS [12] SFE GMNIA, employing validated models employed by the authors in the past (*e.g.*, [9, 13, 14]). The beams are discretised into fine meshes of S4 element (ABAQUS nomenclature – 4-node general-purpose SFE with six degrees of freedom per node and full integration). The analyses (i) were performed by means of an incremental-iterative technique, combining Newton-Raphson's method with an arc-length control strategy, and (ii) simulate the response of beams subjected to constant uniform temperature distributions (*i.e.*, the beams are deemed engulfed in flames, thus sharing the temperature with the surrounding air) and subsequently subjected to an increasing uniform major-axis bending moment up to failure – steady-state structural analyses providing failure moments. The force/moment application is always made in small increments, by means of the ABAQUS automatic loading stepping procedure. All analysed beams contain initial geometric imperfections with a

global critical mode shape and amplitude of $L/1000$. However, beams with a distortional critical mode shape will always be considered purely distortional initial imperfections and amplitude of $0.1t$. The beam critical buckling mode shapes are obtained through preliminary ABAQUS buckling analyses, performed with the SFE mesh subsequently employed to carry out the GMNIA – this procedure makes it easy to "transform" the buckling analysis output into a GMNIA input. It is still worth noting that no strain-hardening, residual stresses and/or corner strength effects were considered.

3.2 Elastic-Plastic Post-Buckling Behaviour

This section addresses the influence of elevated temperatures on the elastic-plastic post-buckling behaviour and failure moment of a representative sample of CFS simply supported (SCA and SCB) lipped channel beams, adopting the EC3:1-2 temperature-dependent steel constitutive model (see [11]). Figs. 2(a)-(b) show equilibrium paths M/M_{crD} *vs.* $|v|/t$ and M/M_{crG} *vs.* $|w|/t$, where t is the wall thickness, $|v|$ and $|w|$ are the absolute values of the beam maximum vertical and horizontal displacements, occurring at the mid-spam compressed (top) flange-lip and flange-web corner, concerning beams with λ_D=1.2 (yield stress $\sigma_{y.20}$ equal to 600 MPa and 840 MPa, respectively for the SCA and SCB support conditions) and λ_G=1.5 (453 MPa and 535 MPa, for SCA and SCB) at temperatures T=100-300-600-800 ºC. The white circles identify the failure moments $M_{u.T}$. As for Figs. 3(a)-(b), they display the deformed configurations and von Mises stress contours, at collapse (M=$M_{u.T}$), of the beams at temperatures T=100-300-600-800 ºC.

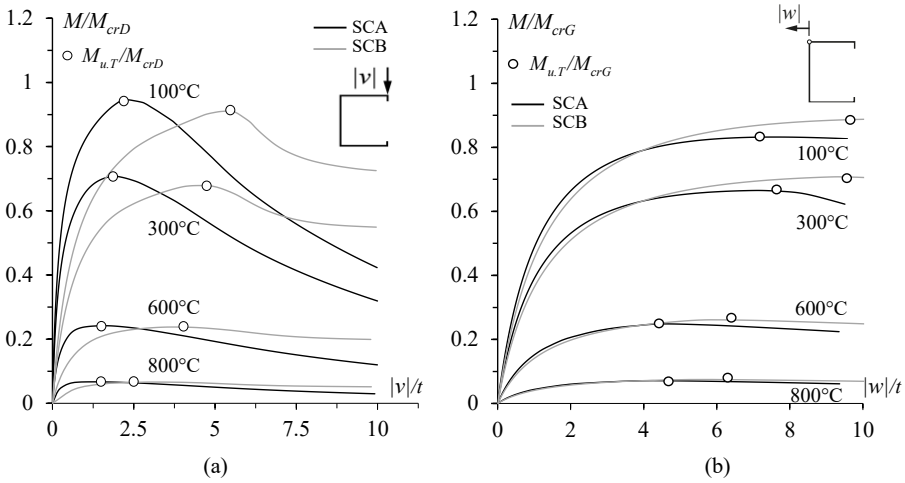


Figure 2. Non-linear equilibrium paths (a) M/M_{crD} *vs.* $|v|/t$ and (b) M/M_{crG} *vs.* $|w|/t$ of SCA and SCB beams with λ_D=1.2 (distortional) and λ_G=1.5 (global) at temperatures T=100-300-600-800 ºC

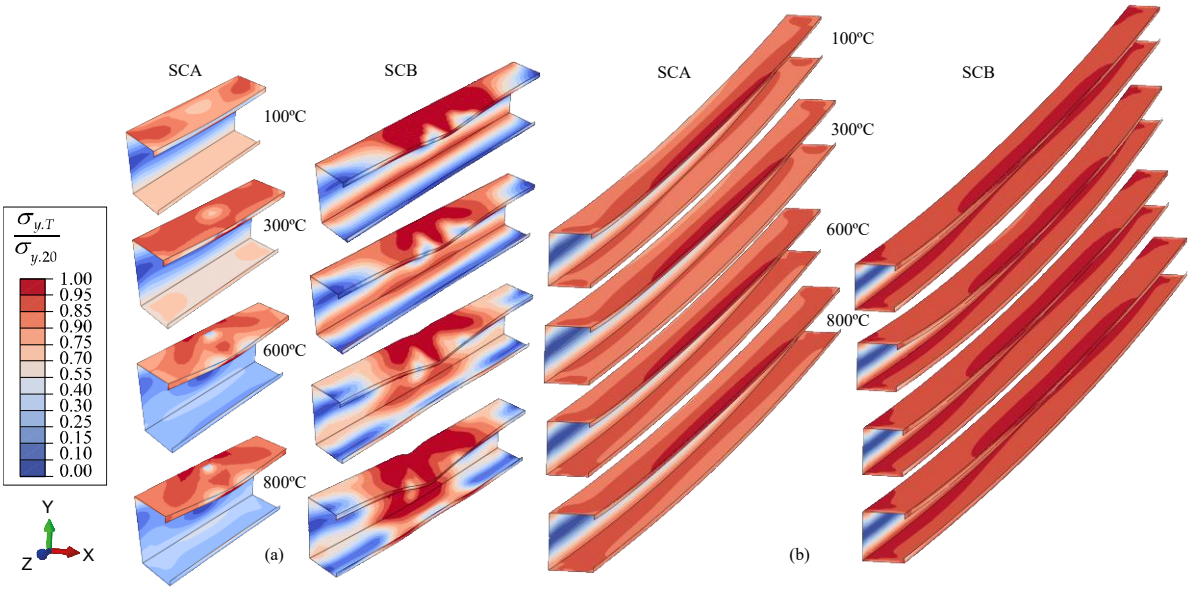


Figure 3. Deformed configurations and von Mises stress contours, at collapse, of the SCA and SCB beams with (a) λ_D=1.2 (distortional) and (b) λ_G=1.5 (global) under temperatures T=100-300-600-800ºC

4 DSM Design at Room and Elevated Temperatures

4.1 DSM Design against Distortional Failures

The DSM design curve prescribed in [4-6], for beams failing in distortional modes at room temperature, was developed and calibrated on the basis of the experimental [15] and numerical [16] failure moment data reported by Yu and Schafer, and is given by the expressions

$$M_{nD} = \begin{cases} M_y + \left(1 - C_{yd}^{-2}\right)\left[M_p - M_y\right] & \lambda_D \le 0.673 \\ M_y\left[1 - 0.22/\lambda_D\right]/\lambda_D & \lambda_D > 0.673 \end{cases} \quad \text{with} \quad \lambda_D = \sqrt{\frac{M_y}{M_{crD}}} \quad , \quad (1)$$

where, (i) M_{crD} and λ_D are the beam distortional critical buckling moment and slenderness, (ii) M_y and M_p are the yield and plastic moments, and (iii) $C_{yd}=(0.673/\lambda_D)^{0.5}\leq 3$ accounts for inelastic strength reserve. In 2016, Landesmann and Camotim [13], in the context of an investigation on the distortional behaviour and design of CFS simply supported lipped channel beams under major-axis bending at elevated temperatures, unveiled the fact that Eq. (1) predicts inadequately the failure moments in the moderate and high slenderness ranges. One year later, Martins *et al.* [7] confirmed the previous findings and, on the basis of an extensive parametric study, proposed novel DSM-based design curves for CFS simply supported beams under uniform bending, cast in the format

$$M_{nD} = \begin{cases} M_y + \left(1 - C_{yd}^{-2}\right)\left[M_p - M_y\right] & \lambda_D \le 0.673 \\ M_y\left[1 - a/\lambda_D^{b}\right]/\lambda_D^{c} & \lambda_D > 0.673 \end{cases} \quad \text{with} \quad \lambda_D = \sqrt{\frac{M_y}{M_{crD}}} \quad , \quad (2)$$

which were shown to clearly outperform Eq. (1). In these curves, (i) the initial ($\lambda_D\leq 0.673$) branch of Eq.(1) remains unchanged and (ii) parameters a, b, c depend on the beam end support conditions (SCA or SCB – see Figs. 1(a)-(b)) cross-section shape and bending axis – in the case of lipped channel beams under major-axis bending their values are a=0.25, b=1.75, c=1.75 (SCA beams) and a=0.23, b=1.55, c=1.45 (SCB beams). Recently, Neves *et al.* [8] proposed a slight change in the SCB beam parameter values (to a=0.25, b=1.51, c=1.52), which further improved the failure moment prediction quality for such beams.

For lipped channel beams at elevated temperatures, Neves *et al.* [14] expanded the scope of earlier work [7, 13] and investigated the post-buckling behaviour, ultimate strength and DSM-based design against distortional failure at elevated temperatures (up to 800°C). They gathered numerical failure moment data concerning 2400 LCB involving (i) 30 geometries, (ii) two support conditions (SCA and SCB), (iii) five yield stresses and (iv) eight uniform temperatures (100-800°C) – these data were obtained for beams whose temperature-dependent steel material behaviour is described by a model based on that prescribed in Part 1-2 of Eurocode 3 [11]. In order to assess the failure moment prediction quality provided by the modified Eq. (2) ($M_{nD.T}$), Fig. 4(a) depicts illustrative $M_{u.T}/M_{nD.T}$ *vs.* $\lambda_{D.T}$ plots, taken from [14] and for LCB at 200, 500 and 800°C – the white and grey dots stand for SCA and SCB beams, respectively. These plots show that just incorporating the temperature dependence, via $M_{y.T}$, $M_{p.T}$ and $M_{crD.T}$, does not suffice to achieve an efficient failure moment prediction for SCA and SCB lipped channel beams at elevated temperatures. Indeed, mostly safe and reasonably accurate failure moment estimates are only obtained for $\lambda_{D.T}\geq 2.0$ – failure moment overestimations occur for the less slender beams, particularly for the most stock ones. Based on this finding, the authors incorporated into the $M_{nD.T}$ design curves (i) the temperature-dependent ratio k_p/k_y (reduction factors prescribed in [11]) and (ii) a coefficient η (ensuring continuity between the two design curve branches and provided in tabular form in [14]), leading to (Eq. (3))

$$M_{nD.T^*} = \begin{cases} \left(M_{y.20}\cdot k_p\right) + \dfrac{\left(1 - C_{yd.T}^{-2}\right)}{\left(k_p/k_y\right)^{2.5}}\left[M_{p.T} - M_{y.T}\right] & \lambda_{D.T} \le 0.673/\eta \\ M_{y.T}\left[1 - a\cdot\left(k_y/k_p\right)/\lambda_{D.T}^{b}\right]/\lambda_{D.T}^{c} & \lambda_{D.T} > 0.673/\eta \end{cases} \quad \text{with} \quad \lambda_D = \sqrt{\frac{M_y}{M_{crD}}} \quad . \quad (3)$$

By comparing the $M_{u.T}/M_{nD.T}$ *vs.* $\lambda_{D.T}$ and $M_{u.T}/M_{nD.T^*}$ *vs.* $\lambda_{D.T}$ depicted in Figs. 4(a) and 4(b), respectively, it is readily observed that the $M_{nD.T^*}$ failure moment estimates clearly outperform their $M_{u.T}/M_{nD.T}$ counterparts, since the failure moment prediction quality significantly improves in low and moderate slenderness ranges. On the other hand, it is also observed that several slender SCB beam failure moments are visibly underestimated.

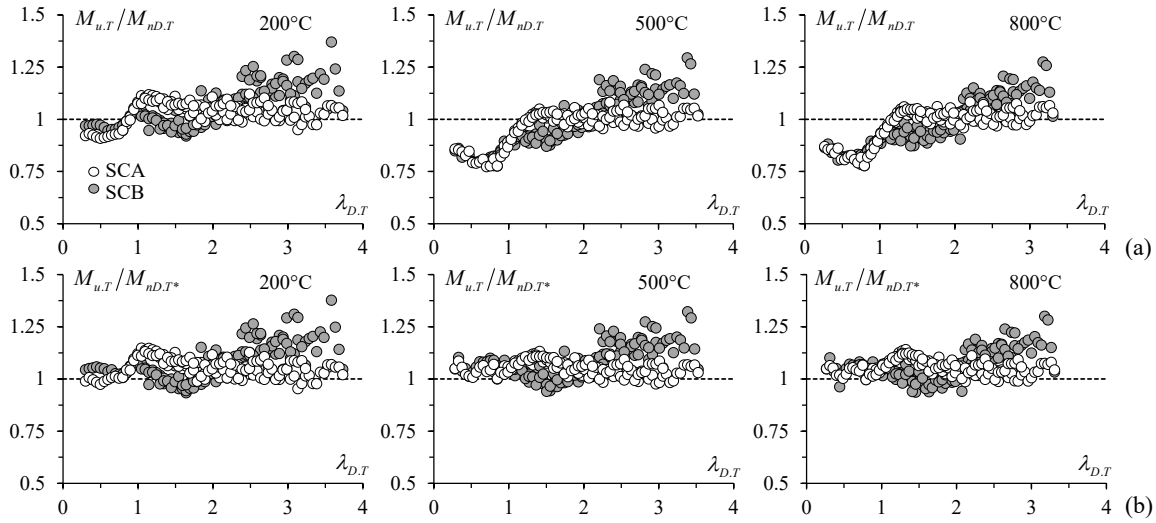


Figure 4. (a) Illustrative $M_{u.T}/M_{nD.T}$ *vs.* $\lambda_{D.T}$ and (b) $M_{u.T}/M_{nD.T*}$ *vs.* $\lambda_{D.T}$ plots of SCA and SCB LCB at T=200, 500 and 800ºC

4.2 DSM Design against Global Failures

The design curve prescribed in [4-6], for beams failing in global (lateral-torsional) modes at room temperature, was (i) first codified about 40 years ago, in the context of hot-rolled steel doubly symmetric I-section beams [17, 18], and (ii) subsequently adopted by the cold-formed steel specifications, namely in the context of the DSM design methodology [4-6]. The failure moment estimates, M_{nG}, are given by

$$M_{nG} = \begin{cases} M_p - \left(M_p - M_y\right)\left[2.70\left(\lambda_G - 0.23\right)\right] & \lambda_G \le 0.60 \\ \dfrac{10}{9} M_y \left(1 - \dfrac{10}{36}\lambda_G^2\right) & 0.60 < \lambda_G < 1.336 \\ M_y \lambda_G^{-2} & \lambda_G \ge 1.336 \end{cases} \quad \text{with} \quad \lambda_G = \sqrt{\frac{M_y}{M_{crG}}} \quad , \quad (4)$$

where (i) M_{crG} and λ_G are the beam global critical buckling moment and slenderness, and (ii) M_y and M_p are the yield and plastic moments. About a decade ago, Kankanamge and Mahendran [19], investigated the behaviour and design of CFS single-span simply supported (SCA) LCB failing in lateral-torsional (LT) modes at room temperature and found that, the codified M_{nG} design curve significantly overestimated the LT failure moments of practically all the beams analysed (with the exception of the very stocky ones). Recently, Neves *et al.* [9] extended the scope of the investigations reported in [8, 19], by analysing much larger sets of CFS LCB (both SCA and SCB beams were considered) at room and elevated temperatures (up to 800 ºC). At room temperature, these authors showed that the design curves prescribed in [4-6, 19] overestimate either virtually all (Eq. (4)) or a visible fraction (proposed curve in [19]) of the available LT failure moment data. This finding prompted Neves *et al.* [9] to propose novel DSM-based design curves to handle LT failures in CFS simply supported (SCA and SCB) lipped channel beams. These strength curves, cast in the same format as the then codified column DSM global design curve [4], are given by the expressions

$$M_{nLT} = \begin{cases} M_p (0.643 \cdot a)^{\lambda_G^{1.5}} & \lambda_G \le 1.5 \\ M_y \left(\dfrac{b}{\lambda_G^2}\right) & \lambda_G > 1.5 \end{cases} \quad \text{with} \quad \lambda_G = \sqrt{\frac{M_y}{M_{crG}}} \quad , \quad (5)$$

where, (i) $a=(bS/Z)^{0.544}$ is a coefficient ensuring continuity of the two design curve branches at λ_G=1.5, and (ii) b is a parameter dependent on the beam end support conditions: b=0.790 and b=0.853, respectively for SCA and SCB beams. The M_{nLT} curves were shown to adequately predict the LT failure moments of all the SCA and SCB LCB analysed in [8, 9]. At elevated temperatures, Neves *et al.* [9] showed that the curve proposed by [8] consistently yield failure moment overestimations, except for beams at T=200 ºC within a narrow intermediate slenderness band – in fact, and a bit surprisingly, this overestimation also occurs for the failure moments obtained by the authors who proposed these strength curves [8]. This finding prompted Neves *et al.* [9, 20] to improve the failure moment prediction quality provided by the curve proposed by [8], which was done through the development of novel DSM-based design curves (i) based on Eq. (5) and (ii)

incorporating, in the first branch ($\lambda_{G.T} \leq 1.5$), temperature-dependent parameters able to account for both the EC3:1-2 [11] and AS/NZS 4600 [5] CFS constitutive models – it is termed $M_{nLT.T*}$ and reads

$$M_{nLT.T*} = \begin{cases} M_{p.T}\left(\varphi_T \dfrac{k_p}{k_y}\right) a^{\lambda_{G.T}^c} & \lambda_{G.T} \leq 1.5 \\ M_{y.T}\left(\dfrac{b}{\lambda_{G.T}^2}\right) & \lambda_{G.T} > 1.5 \end{cases} \quad \text{with} \quad \lambda_{G.T} = \sqrt{\frac{M_{y.T}}{M_{crG.T}}} \quad , \quad (6)$$

where (i) $a = (0.444b \cdot S/Z \cdot k_y/k_p \cdot \varphi_T)^{1.5-c}$ is temperature-dependent (via k_y/k_p, φ_T and c), (ii) b remains the same as in Eq. (5)) and (iii) the values of c and φ_T, tabulated in [20], differ for the EC3:1-2 [11] and AS/NZS 4600 [5] CFS constitutive models. Figs. 5(a)-(b) illustrative $M_{u.T}/M_{nLT.T*}$ *vs.* $\lambda_{G.T}$ plots, taken from [9] (EC3:1-2 CFS constitutive model) and [20] (AS/NZS 4600 CFS constitutive model), concerning LCB at 200, 500 and 800°C – the white and grey dots stand for the SCA and SCB beams, respectively. The whole set of plots included in [9, 22] provide clear evidence of how efficiently (safely, accurately and reliably) Eq. (6) handles the LT failures of simply supported (SCA and SCB) lipped channel beams (i) uniformly bent about the major axis, (ii) at both room and elevated temperatures (up to 800°C), and (iii) exhibiting temperature-dependent CFS material behaviours prescribed by either the EC3:1-2 [11] or AS/NZS 4600 [5] constitutive models.

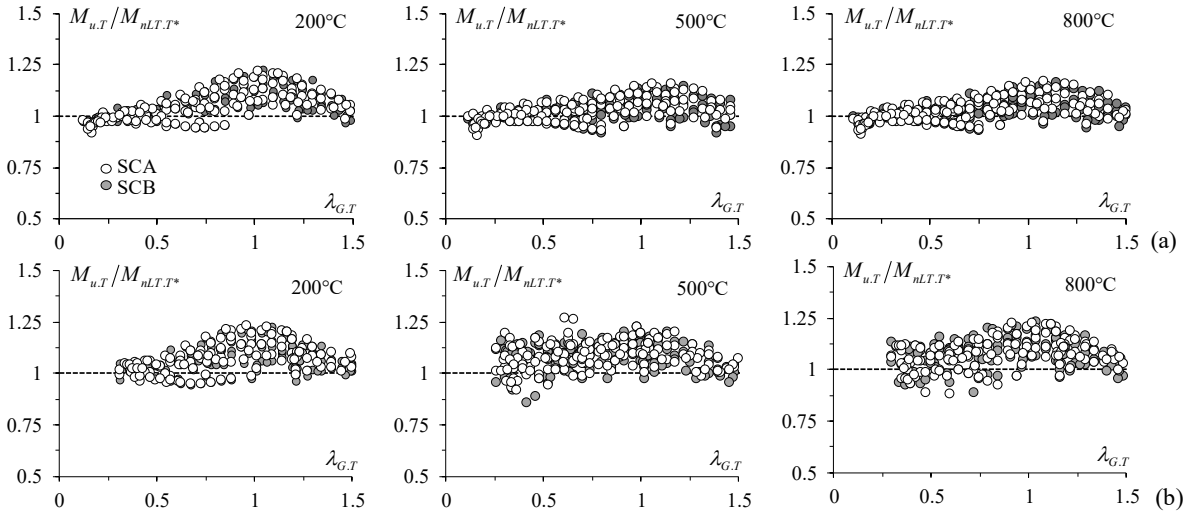


Figure 5. Illustrative $M_{u.T}/M_{nLT.T*}$ *vs.* $\lambda_{G.T}$ plots of SCA and SCB CFS LCB at T=200, 500 and 800ºC with material behaviours described by the (a) EC3:1-2 [9] and (b) AS/NZS 4600 [20] constitutive models.

5 Conclusions

This paper reported the most recent results of an ongoing investigation on the post-buckling behaviour, ultimate strength and Direct Strength Method (DSM) design of cold-formed steel (CFS) single-span simply supported lipped channel beams failing in distortional and global modes at elevated temperatures, typically caused by fire conditions. Extending earlier studies, this work considered a broader range of cross-section geometries and slenderness levels, along with two end support conditions (SCA and SCB), in order to assess the reliability of existing DSM-based design curves. It was found that the codified DSM distortional strength curve performs poorly at elevated temperatures, as expected, and that the more recent curves proposed by Martins *et al.* [9] still lead to non-conservative predictions, especially for beams with low to moderate distortional slenderness. To address this limitation, the distortional design curve was modified by incorporating temperature-dependent parameters, namely the ratio k_p/k_y, and the coefficient η. This modification led to a significant improvement in prediction quality, enabling safe and accurate failure moment estimates over a wide slenderness range. These promising results suggest that the adopted approach provides a solid foundation for developing an efficient DSM-based design framework capable of handling arbitrary CFS beams failing in distortional and global modes at elevated temperatures.

Acknowledgements. The first two authors gratefully acknowledge the financial support of the Brazilian institutions (i) CAPES (Coordenação de Aperfeiçoamento de Pessoal de Nível Superior) – Finance Code 001 (both authors), and (ii) CNPq (Conselho Nacional de Desenvolvimento Científico e Tecnológico) – Finance Codes 141021/2020-9 (first author) and 313197/2020-2 (second author). The third author gratefully acknowledges the financial support of FCT (Fundação para a Ciência e a Tecnologia – Portugal) – project UIDB/04625/2020 (funding the research unit CERIS).

Authorship statement. The authors hereby confirm that they are the sole liable persons responsible for the authorship of this work, and that all material that has been herein included as part of the present paper is either the property (and authorship) of the authors, or has the permission of the owners to be included here.

References

[1] Camotim D, Dinis PB, Martins AD (2016). Direct Strength Method (DSM) – a general approach for the design of cold-formed steel structures, *Recent Trends in Cold-Formed Steel Construction*, C. Yu (ed.), Woodhead Publishing, Amsterdam, 69-105.

[2] Schafer BW (2019). Advances in the Direct Strength Method of cold-formed steel design, *Thin-Walled Structures*, **140**(July), 533-541.

[3] Camotim D, Martins AD, Dinis PB (2023). Towards the next generation design of cold-formed steel structures: the Direct Strength Method (DSM), *Recent Trends in Cold-Formed Steel Construction* (2nd edition), C. Yu (ed.), Woodhead Publishing (Series in Civil and Structural Eng.), Elsevier, Cambridge (MA – USA) and Kidlington (UK), 101-173.

[4] AISI (American Iron and Steel Institute) (2022). *North American Specification (NAS) for the Design of Cold-Formed Steel Structural Members* (2016 edition reaffirmed in 2020 with Supplement 3), AISI-S100-16 w/S3-22, Washington DC.

[5] AS/NZS (Standards of Australia and Standards of New Zealand) (2018). *Cold-Formed Steel Structures*, AS/NZS 4600:2018 (3rd ed.), Sydney-Wellington.

[6] ABNT (Brazilian Standards Association) (2010). *Brazilian Standard on Design of Cold-Formed Steel Structures*, ABNT NBR 14762:2010, Rio de Janeiro. (Portuguese).

[7] Martins AD, Landesmann A, Camotim D, Dinis PB (2017). Distortional failure of cold-formed steel beams under uniform bending: Behaviour, strength and DSM design, *Thin-Walled Structures*, **118**(September), 196-213.

[8] Kankanamge ND, Mahendran M (2012). Behaviour and design of cold-formed steel beams subject to lateral-torsional buckling at elevated temperatures, *Thin-Walled Structures*, **61**(December), 213-228.

[9] Neves NS, Landesmann A, Camotim D (2025). Lateral-torsional failure and DSM design of CFS lipped channel beams at room and elevated temperatures, *Thin-Walled Structures*. **209**(April), paper 112520.

[10] Bebiano R, Camotim D, Gonçalves R (2018). GBTul 2.0 – a second-generation code for the GBT-based buckling and vibration analysis of thin-walled members, *Thin-Walled Structures*, **124**(March), 235-257.

[11] CEN (Comité Européen de Normalisation) (2005). *Eurocode 3: Design of Steel Structures – Part 1.2: General Rules – Structural Fire Design*, EN 1993-1-2, Brussels.

[12] Simulia Inc. (2014). *ABAQUS Standard* (version 6.14-1).

[13] Landesmann A, Camotim D (2016). Distortional failure and DSM design of cold-formed steel lipped channel beams under elevated temperatures, *Thin-Walled Structures*, **98A**(January), 75-93.

[14] Neves NS, Landesmann A, Camotim D (2024). CFS lipped channel beams buckling in distortional modes at elevated temperatures: behaviour, failure and DSM design, *Thin-Walled Structures*, **195**(February), paper 111366.

[15] Yu C, Schafer BW (2006). Distortional buckling tests on cold-formed steel beams, *Journal of Structural Engineering* (ASCE), **132**(April), 515-528.

[16] Yu C, Schafer BW (2007). Simulation of cold-formed steel beams in local and distortional buckling with applications to the direct strength method, *Journal of Constructional Steel Research*, **63**(May), 581-590.

[17] AISC (American Institute of Steel Construction) (1986). *Load and Resistance Factor Design Specification for Structural Steel Buildings*, AISC 328:1986, Chicago IL.

[18] Galambos TV (1963). Inelastic Buckling of Beams, *Journal of the Structural Division* (ASCE), **89**(ST5), 217-244.

[19] Kankanamge ND, Mahendran M (2012). Behaviour and design of cold-formed steel beams subject to lateral-torsional buckling, *Thin-Walled Structures*, **51**(February), 25-38.

[20] Neves NS, Landesmann A, Camotim D (2025). DSM-based prediction of lateral-torsional failure of cold-formed steel lipped channel beams at elevated temperatures: influence of the constitutive model, *submitted for publication*.